Project Work

Introduction to Nuclear Engineering

Modeling of decay heat removal system

EHRS loop at Siet Lab in Piacenza

Akzhol Almukhametov, Lorenzo Mazzocco, Lorenzo Meucci,
Daniele Timpano, Patrik Shytaj, William Oliveira

December 2021

Contents

1 Introduction

In any nuclear power production application technology we deal with high thermal power within the reactor core. Following a SCRAM procedure for shutting down the operation of a reactor, the main focus is too keep cooling down the reactor core, whose thermal power from the decay heat of fission products amounts at roughly 6 % of the nominal thermal power.

There are different ways of addressing this problem: with the use of active safety systems we rely on electricity to run machines that pump cold liquid in the core, whereas passive safety systems employ physical laws to address decay heat removal. The lack of mechanical moving parts or other active components should reduce the probability of hardware failure. Passive safety systems rely on natural circulation loops which are meant to work off-grid ensuring a high-level of safety even in severe accident scenarios.

The IES facility (IRIS EHRS Simulator) in Siet Lab (Piacenza) is a **natural circulation** and **electrically heated** loop, with a helical coil steam generator as a *heat source* and a tube pool condenser as a *heat sink*. It was meant to address the key parameters and oscillations of a DHRS for a integral-PWR design, that of the IRIS reactor. The following MATLAB code stems for modelling this loop in a **steady-state condition**.

2 Balance equations and assumptions

All the equations used are derived for steady-state working conditions and are here written in integral form:

Mass Balance:

$$\dot{m} = const$$

Energy Balance:

$$\dot{Q}_{heater} + \dot{Q}_{condenser} = \dot{m} \int_{loop} dh = 0$$

Momentum Balance:

$$\int_{loop} \Phi_l^2 \frac{f_l (1-x) G_m^2}{2D\rho}\, dl \;+\; \sum_j K_j \frac{G^2}{2\rho} = \int_{downcomer} \rho g\, dz - \int_{riser} \rho g\, dz$$

The assumptions we made to model the physical evolution of the fluid around the loop are the following:

- the fluid was modelled according to the **Homogeneous Equilibrium Model** (HEM), so both the same pressure and temperature are shared by the saturated liquid and vapor in the two-phase mixture;
- the system was considered **adiabatic**, with **no heat losses** along the loop;
- the effects of **frictional** pressure drops on the energy balance of the fluid were considered negligible;
- the **frictional pressure drops** for two-phase flow mixture are calculated considering a separated fluids model by means of the **Lockhart-Martinelli correlations**;
- the **frictional** pressure drops in the **condenser** are **negligible**;

3 Physical Model

The whole experimental facility is divided into 6 elements for modelling purposes. The figure above illustrates how the thermodynamic coordinates were labelled around the loop.

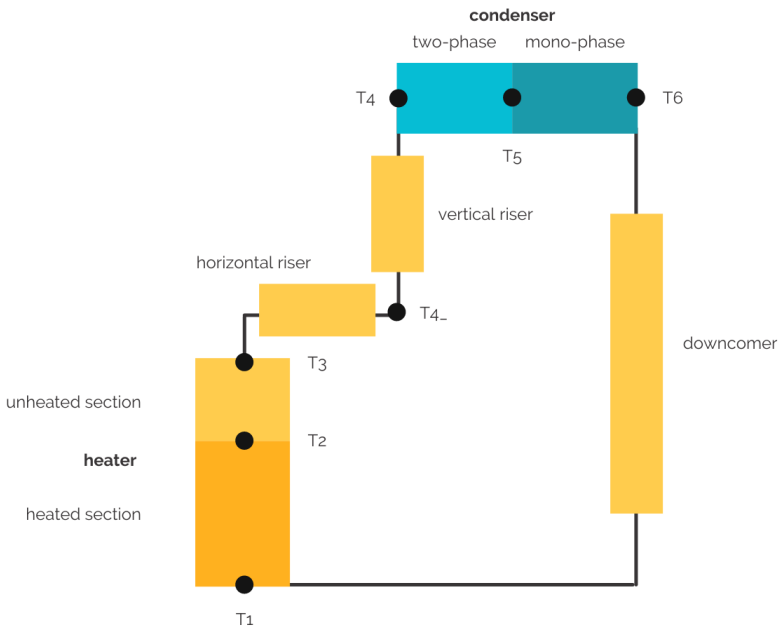

For modeling purposes the heater was divided into a heated and an unheated section [T1 - T2 - T3], the riser is composed by an horizontal [T3 - T4_] and a vertical section [T4_ - T4], the condenser gets a two-phase flow mixture which is firstly condensed in a variable length section [T4 - T5] and then turns into sub-cooled liquid in the second part [T5 - T6].

Knowing the whole geometry and characteristics of the loop, the **inputs** necessary to run a simulation are the thermodynamic coordinates at the inlet of the heater (point 1), the power exchanged to the fluid by the heater and the mass flow rate of the fluid. Of those inputs just two (power exchanged by the heater and inlet pressure) can be decided, from those conditions the loop then finds a steady state equilibrium of natural circulation determining the temperature at the inlet of the heater and the mass flow rate. In order to select sets of inputs that actually create a steady state condition we need to apply an iterative convergence algorithm (see section 4).

The two main physical phenomena to simulate around the loop are: pressure drops and heat transfer in the condenser. Those two phenomena are modelled using apposite modules called **biphase_pressure_drops** and **condensation** respectively.

3.1 Distributed pressure drops module

This module is applied to the following elements around the loop: heated and unheated heater, horizontal riser, vertical riser.

Both the pipe length and height are discretized in N (N=100) steps. At every step the condensated liquid fluid frictional and gravitational pressure drops are computed using the fluid properties at the beginning of the discretization step. It is checked if the fluid enters the step as a biphase mixture or a condensated liquid. If the fluid enters as a biphase mixture the corrective coefficient for biphase pressure drops Φ_l^2 is computed. Once the total pressure drop is computed for the step the fluid properties are updated for the next step. Furthermore heat exchange with the environment is contemplated, the only input needed is the heat flux q"

considered constant over the whole length of the pipe.

The approach taken makes it possible to use this module for pressure drops in the heater (both heated and unheated sections), for the riser and downcomer. Moreover checking of the biphase state at every discretization step makes it possible to simulate phenomena such as evaporation in the heater or riser using the same module for both monophase and biphase pressure drops.

Two-phase pressure drops were computed using the separated fluids model by means of the Lockhart-Martinelli correlation. In particular the following equations were used to compute pressure drops at every step of the discretization:

Always: $\Delta p = \Delta p_{friction} + \Delta p_{gravitational}$

Monophase: $\Delta p = -\frac{fLG^2}{2D\rho} - \rho g \Delta z$

Two-phase: $\Delta p = -\Phi_l^2 \frac{f_l L(1-x)G_m^2}{2D\rho} - \rho_m g \Delta z$

with $\Phi_l^2 = 1 + \frac{12}{X} + \frac{1}{X^2}$, $X^2 = (\frac{1-x}{x})^{1.8}(\frac{\rho_v}{\rho_l})(\frac{\mu_l}{\mu_v})^{0.2}$

where the subscripts m, l, v stand for *mixture*, *saturated liquid*, *saturated vapour* and G is the mass flux. [1]

3.2 Concentrated pressure drops

Around the loop concentrated pressure drops are very much simplified since their influence on the overall momentum balance are minor. Nevertheless concentrated pressure drops are computed at the inlet and outlet of the heater, in the riser and in the downcomer.
The formula used to compute them is :

$\Delta p = -K\frac{G^2}{2\rho}$, with a default value of K=2.

3.3 Condensation module

Heat transfer is simulated using appropriate correlations. The length of the pipe is discretized in multiple steps computing the fluid properties, global heat transfer coefficient and power exchanged at every step. The condenser is divided into two parts: the initial length with a biphase mixture and the final lenght with condensated liquid.

It can be proven that the bulk temperature and global heat transfer coefficient in the biphase region stay constant up to the condensation of the mixture. For this reason the heat transfer in the biphase region is computed discretizing this section of the pipe in one single step with a length such that at the end of the step the liquid is at saturated conditions.

In the liquid region of the condenser the temperature and global heat transfer coefficient vary sensibly with the fluid properties. For this reason heat transfer in this region is simulated discretizing the length of the condenser in N (N=20) steps.

Heat transfer was modelled considering the thermal resistances of convection between the fluid and the inner pipe and the conduction of the pipe. The main assumption was that the outer temperature of the pipe stays fixed at 100°C (no film boiling in the pool around the pipe). The following equations were used:

$\dot{Q}_{cond} = \int_{condenser} \frac{T_{wall}-T_{sat}}{R_{th,tot}}$, where $R_{th,tot} = \frac{1}{\alpha_{conv} A_{in}} + \frac{ln(\frac{R}{r})}{2\pi k L}$

In order to find the convection heat transfer coefficients (α_{conv}) the following correlations were used:

[1] TODREAS, Neil E.; KAZIMI, Mujid S. Nuclear systems volume I: Thermal hydraulic fundamentals. CRC press, 2021.

- **Condensation:** (Chato): $\alpha_{cond} = 0.555[\frac{g(\rho_l - \rho_v)\rho_v K_V^3 h^*_{evap}}{D\mu_l(T_{sat} - T_{wall})}]^{\frac{1}{4}}$
  valid for $Re_v = \frac{G_v D}{\mu_v} < 35000$
- **Subcooling:** (Dittus-Boelter as introduced by McAdams): $Nu = 0.023 Re^{0.8} Pr^{0.3}$
  valid for $0.7 < Pr < 100$, $Re > 10000$ [2]

4 Iterative Algorithm

In order to run a simulation and characterize all the thermodynamic states of the fluid around the loop we need the following inputs: p_1, T_1, $\dot{Q}_{heater}$, $\dot{m}$. Of those we can only control p_1 and $\dot{Q}_{heater}$, the other two are derived from the steady-state equilibrium that the loop reaches.

In order to find T_1 and $\dot{m}$ that create a steady state equilibrium given p_1 and $\dot{Q}_{heater}$ we need to iterate different values until we find the right ones. In particular a two nested loops iterative routine was created which verifies momentum and energy balance. A schematic of such algorithm is given below:

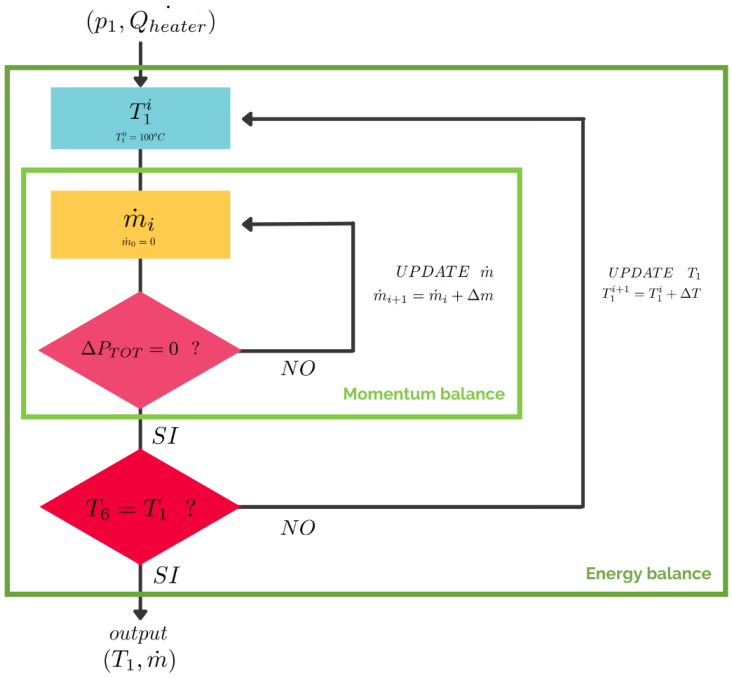

Two loop structure for computing thermodynamic properties

[2] INCROPERA, Frank P., et al. Fundamentals of heat and mass transfer. New York: Wiley, 1996.

5 Results and discussion

236 combinations of power and pressure were simulated. For each simulation that converged to a steady state equilibrium more than 2050 data points are obtained. A total of around 500.000 data points were produced. In Appendix A are tabulated the most interesting quantities from every simulation.

The results show good agreement with the experimental results discussed in *Experimental Characterization of a Passive Emergency Heat Removal System for a GenIII+ Reactor* (Santini et al.) [3]. Following are discussed the most noteworthy results obtained by the model and how they relate to the experimental data.

5.1 Loop working region

In the work by Santini et al. a loop theoretical working region is constructed by limiting the FR in a specific range for a given value of pressure. Said range is identified by a theoretical FR_{max} and FR_{min}. By plotting the values of theoretical FR (derived with the empirical correlation) and system pressure we can identify the working region by differentiating the color of initial conditions that led the algorithm to converge to a steady state equilibrium (green) from those who didn't (red).

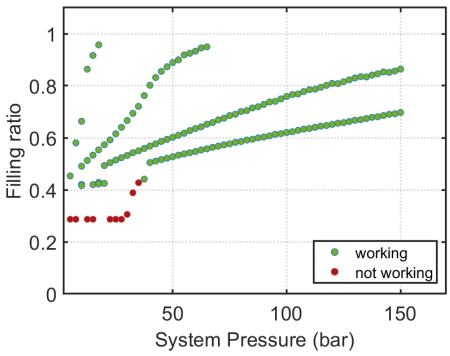

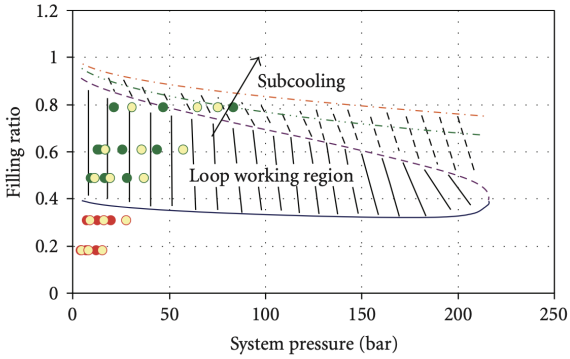

This graph is in excellent agreement with the results obtained by Santini et al. which are plotted on the right for a comparison (figure 7 in the original paper). Both the charts identify the lower boundary of the working region as a filling ratio of around 0.4. Also higher filling ratios are associated with greater subcooling of the water in the condenser as showed by the figure below.

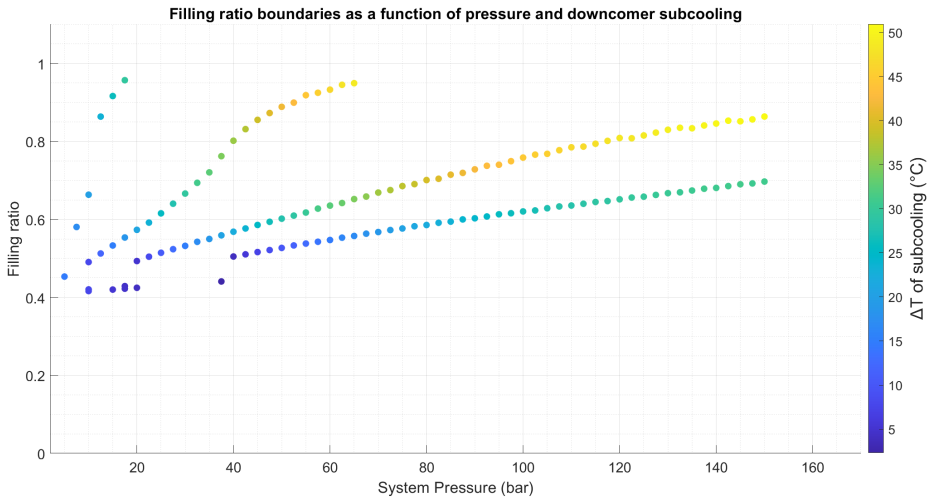

[3] SANTINI, Lorenzo; PAPINI, Davide; RICOTTI, Marco E. Experimental characterization of a passive emergency heat removal system for a GenIII+ reactor. Science and Technology of Nuclear Installations, 2010, 2010

5.2 Effects of filling ratio and pool rejected power

Santini et al. derived a simple correlation for the power rejected to the pool (Q) and the system FR:

$$\frac{p^{0.7}}{T_{sat}} \frac{\Delta h_{lg}}{Q^{0.86}} = 136 \cdot FR^2 - 78 \cdot FR + 49$$

Our model is able to effectively reproduce the relationship between Q, p and FR for a wide range of initial conditions. The following chart plots the trends of pressure vs pool rejected power for different filling ratios (0.49, 0.61 and 0.79) obtained by our model and compares them with the trends set by the correlation constructed by Santini et al. (dotted lines).

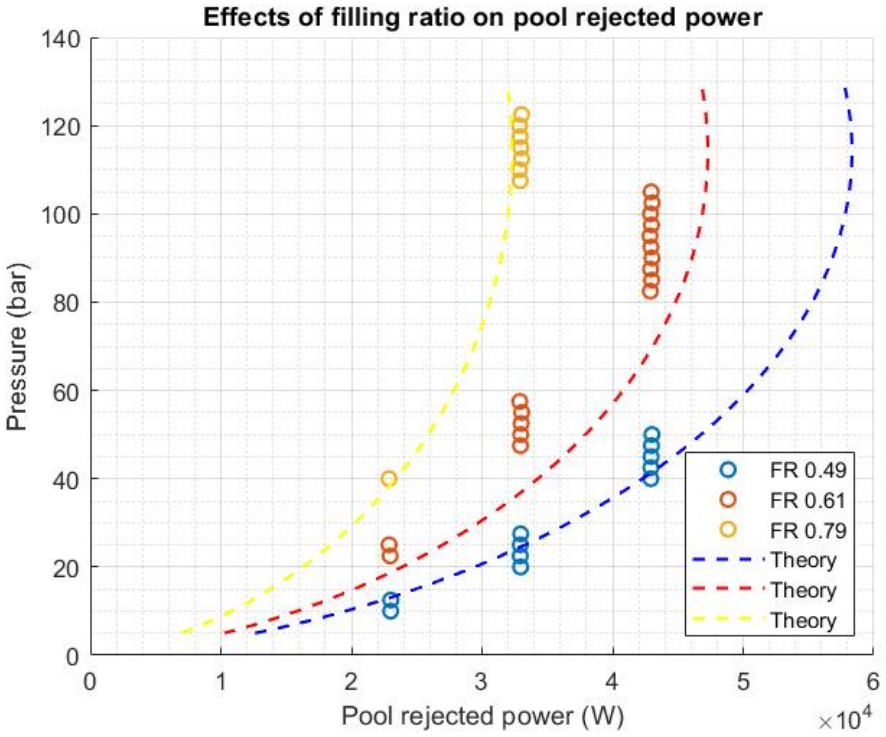

The necessary increase in system pressure from lower to higher FRs is connected to the results discussed in *Section 5.5*. **Higher FRs** result in shorter biphase lengths in the condenser and therefore lower heat transfer coefficients. In order to ensure the heat exchange in the condenser, an increase in ΔT_{ln} is needed, thus causing the need for **higher system pressures**.

5.3 Effects of filling ratio and power on pool condenser outlet subcooling

The relationship between outlet subcooling, power and filling ratio is represented in the paper by Santini et al. in figure 4. Our model is able to reproduce the increase of outlet subcooling for higher filling ratios as shown in the figure below. Nevertheless the relationship between outlet subcooling and power for the same FR is exactly the opposite of the one presented in the paper.

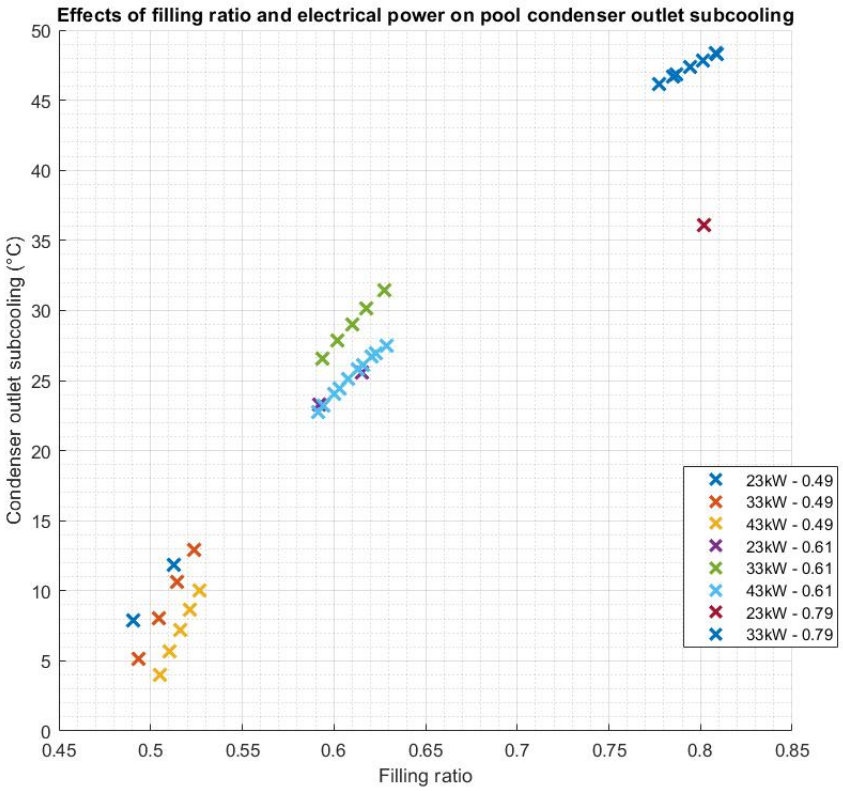

This major difference could be caused by the fact that the data presented by Santini et al. refers to experiments withouth heat losses compensation while **our model neglects heat losses**. Higher power in the heater could cause the enhancement of heat losses in the riser and thus a reduction of the enthalpy that translates in lower temperatures of the fluid at the outlet of the condenser. Following is the image for experimental results without heat losses compensation.

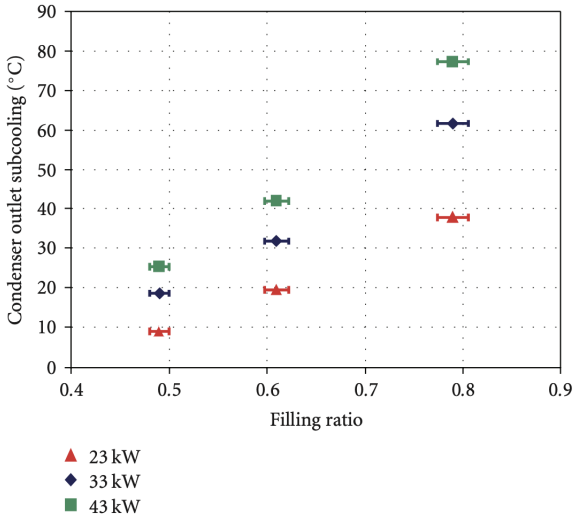

5.4 Effects of filling ratio and power on loop flowrate

The dependency of the **mass flow rate on filling ratio** and power is not monotonic and the reason of this is to be found in the relationship between momentum balance and the single phase zone length of the steam generator as explained by Santini et al. Our model is able to reproduce this complex dependency with a good degree of accuracy. The following chart summarizes our results.

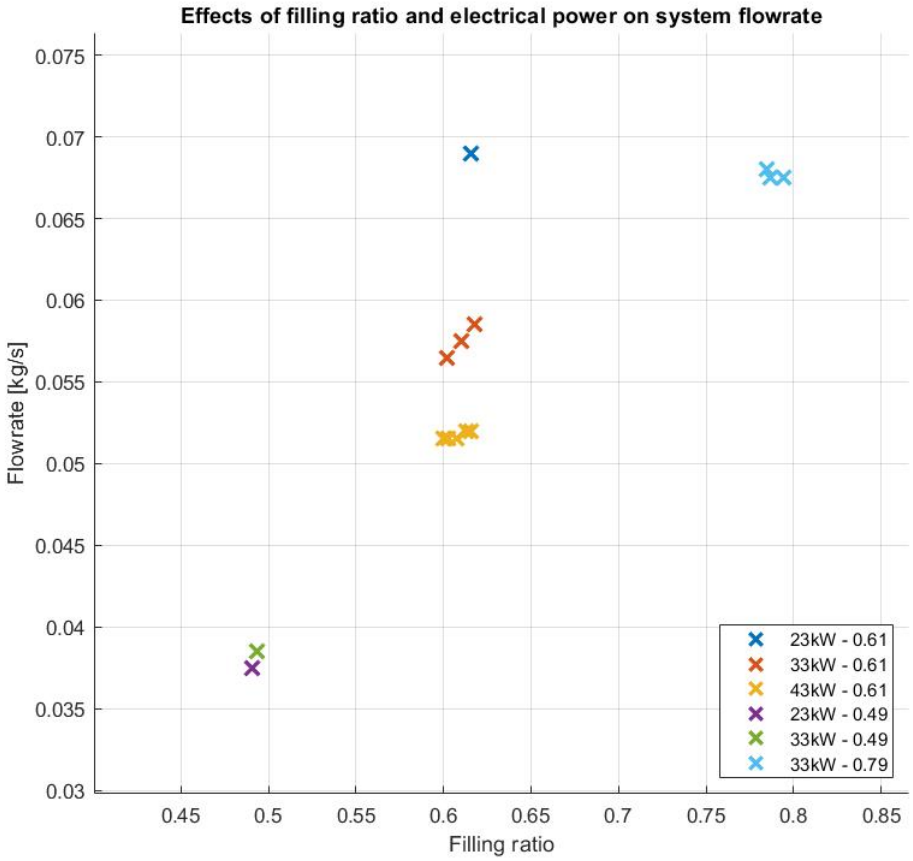

The only difference with the experimental results is that the **critical filling** ratio at which the dependency of the flow rate from the power reverses is **slightly lower** than the experimental one. In our model we can observe the reversal already from a FR of 0.61. Following the experimental results are plotted for the same powers and filling ratios.

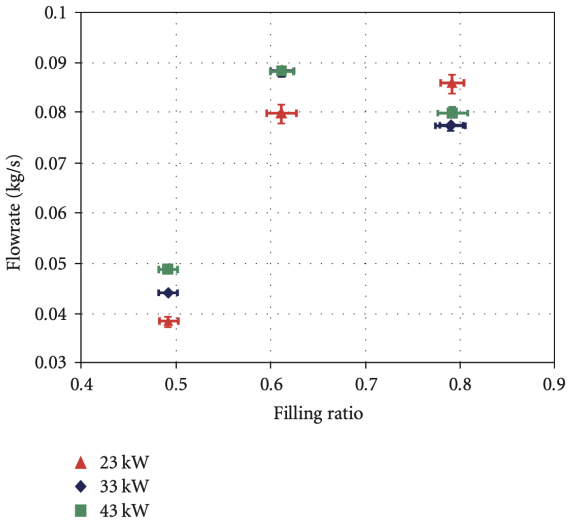

5.5 Effects of filling ratio on two-phase zone length in condenser

Santini et al. explained how an increase of filling ratio, and thus of mass content of the loop, brings the necessity to allocate the increase in mass in the single phase zone lengths of the steam generator and condenser. We are able to confirm these experimental results with the data from our simulations.

For the **condenser** the length of the two-phase zone is clearly decreasing with an increment of filling ratio as shown in the plot below.

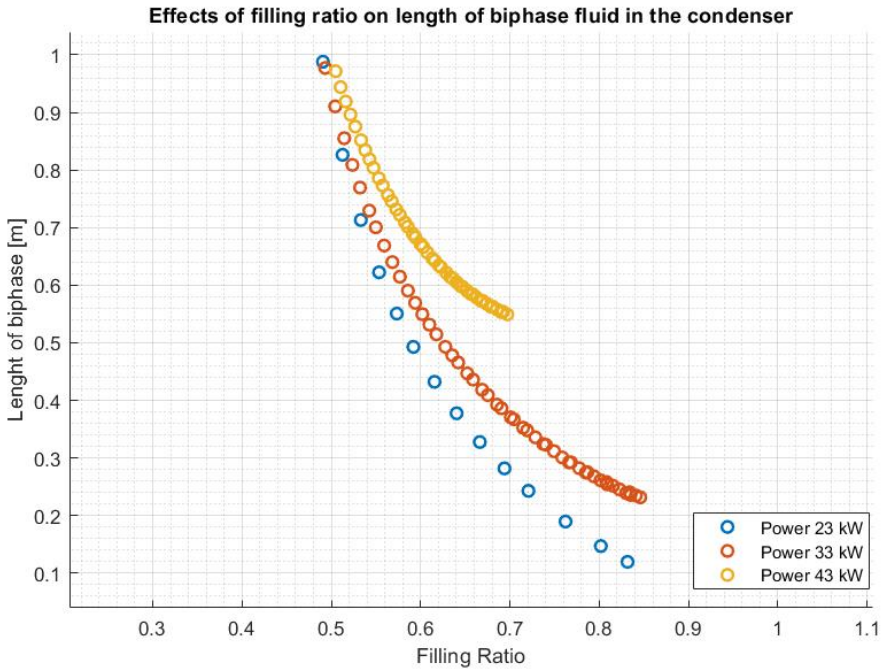

Also in the **steam generator** plotting the density as a function of position in the pipe for different FRs we can see that the single phase zone stretches for higher filling ratios.

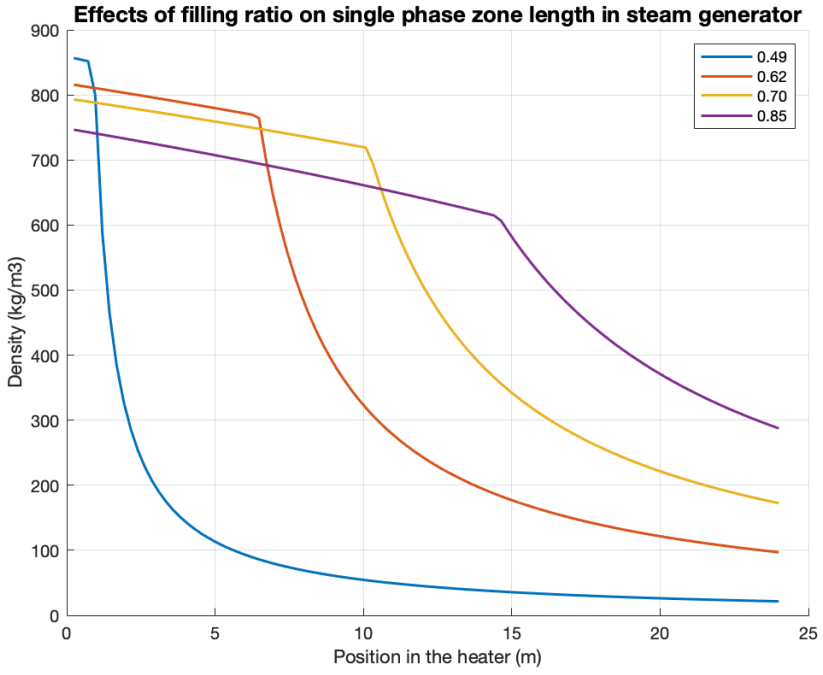

5.6 Stability analysis and oscillations

Although our model was designed and implemented to perform analyses of steady states the fundamental physics implemented in the code can be used to extract information about stability of the equilibrium using characteristic curves as Yang et al. have proposed for similar problems. The modelling of sophisticated two-phase frictional pressure drops correlations make it possible for our model to obtain complex characteristic curves for pressure drops.

The large majority of converged steady states that were simulated showed theoretical stability with characteristic curves similar to the one below (p_1=145b, T_1=289°C, Q=33 kW) with just one intersection point between pressure drops and positive head (pressure gains).

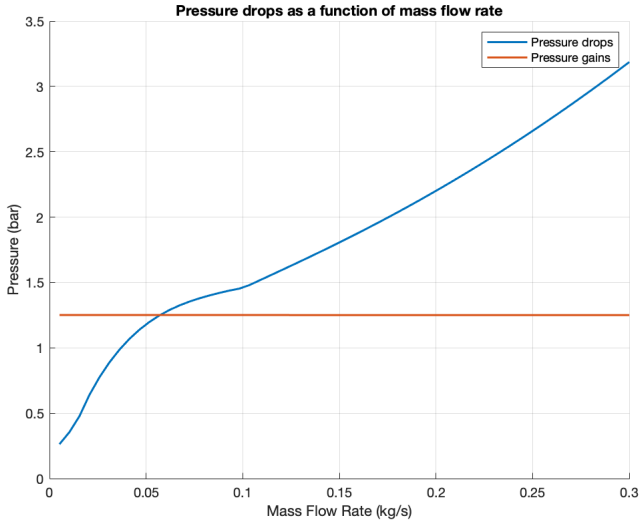

But we can see that under specific conditions (that do not correspond to converged steady state) like p_1=10b, T_1=140°C, Q=23kW we obtain multiple mass flow rate values that solve for momentum balance.

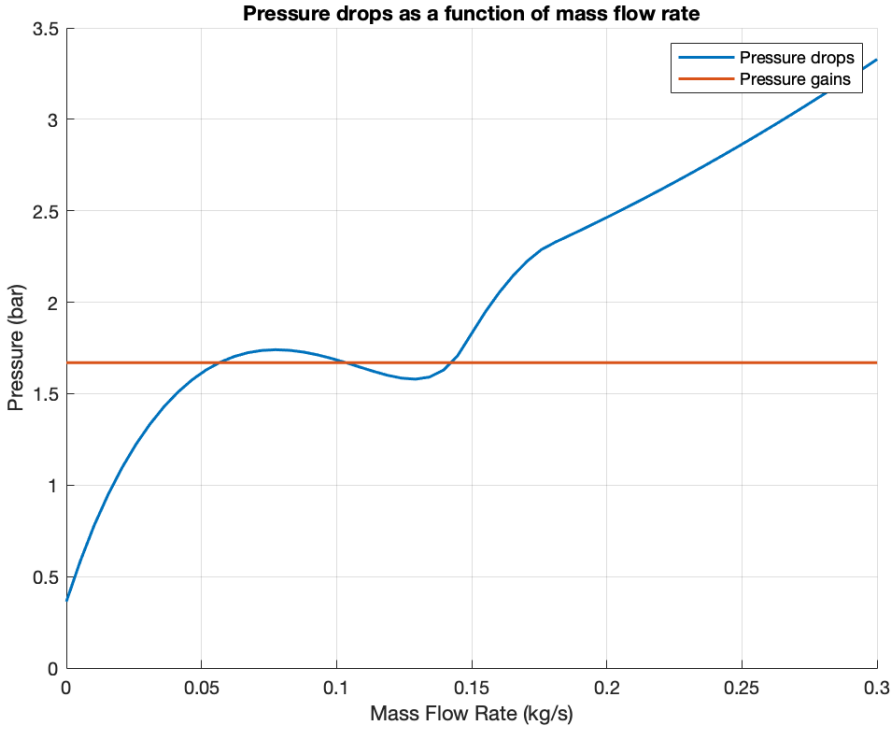

6 Future developments

The model developed on the occasion of the project work activity for the Introduction to Nuclear Engineering course proved solid consistency and adherence to the experimental results presented by Santini et al.

The code modules for pressure drops computation, momentum balance check and heat exchange in the condenser by means of discretization and iteration may be easily adapted to limit the need for simplifying assumptions with regards to:

- **heat losses throughout the loop:** further research concerning heat transfer relations in all the system's components could be integrated in the code, getting rid of the adiabatic assumptions made so far and predicting more coherent results. Experimental data concerning heat losses in the facility could guide this part of the modeling;
- **geometry accuracy:** within the current model elbows and other geometrical peculiarities of the loop have been neglected thus causing an underestimation of the loop volume and concentrated pressure drops. While this version of the code has proven very effective in predicting physically meaningful results, including a complete enquiry on the geometrical features of the EHRS loop in Siet facilities could provide a further degree of accuracy;
- **noncondensable gases content** has been neglected so far. Further investigation on their influence on heat transfer and pressure drops could represent an interesting sensitivity analysis to be carried out;
- **stability analysis and oscillations:** the modeling of the dynamic behaviour of the loop has started using Modelica and it will eventually give us more information concerning loop transients.

7 References

- SANTINI, Lorenzo; PAPINI, Davide; RICOTTI, Marco E. Experimental characterization of a passive emergency heat removal system for a GenIII+ reactor. Science and Technology of Nuclear Installations, 2010, 2010.
- JUHN, P. E., et al. IAEA activities on passive safety systems and overview of international development. Nuclear Engineering and Design, 2000, 201.1: 41-59.
- DING, Hao, et al. Development of a model for thermal-hydraulic analysis of helically coiled tube once-through steam generator based on Modelica. Annals of Nuclear Energy, 2020, 137: 107069.
- TODREAS, Neil E.; KAZIMI, Mujid S. Nuclear systems volume I: Thermal hydraulic fundamentals. CRC press, 2021.
- INCROPERA, Frank P., et al. Fundamentals of heat and mass transfer. New York: Wiley, 1996.

A Appendix: Simulation Results Table

p_1	Q	FR_theory	SS	FR_computed	m_dot	dT_subcooling	x_4	T_1	L_biphase
5	13000	0,47	1	0,45	0,048	0	0,1257	137	1,000
7,5	13000	0,62	1	0,58	0,072	17	0,0708	150	0,561
10	13000	0,71	1	0,66	0,106	20	0,0338	160	0,314
12,5	13000	0,77	1	0,86	0,138	23	0,0085	166	0,088
15	13000	0,82	1	0,92	0,122	26	0,0069	172	0,057
17,5	13000	0,86	1	0,96	0,106	29	0,0057	176	0,037
20	13000	0,89	1	0,97	0,096	32	0,0052	180	0,028
22,5	13000	0,92	1	0,98	0,089	35	0,0048	184	0,023
25	13000	0,95	1	1,00	0,082	37	0,0044	187	0,018
27,5	13000	0,97	1	1,00	0,075	40	0,0039	189	0,014
30	13000	0,99	1	1,01	0,071	42	0,0038	192	0,012
32,5	13000	1,01	1	1,01	0,066	44	0,0036	194	0,010
35	13000	1,03	1	1,02	0,063	46	0,0032	196	0,009
37,5	13000	1,05	1	1,02	0,060	48	0,0031	198	0,007
40	13000	1,06	1	1,03	0,058	50	0,0019	200	0,004
42,5	13000	1,08	1	1,03	0,055	52	0,0025	202	0,005
45	13000	1,09	1	1,03	0,054	53	0,0015	204	0,003
47,5	13000	1,10	1	1,03	0,052	55	0,0011	206	0,002
50	13000	1,11	1	1,03	0,050	57	0,0017	207	0,003
52,5	13000	1,12	1	1,04	0,049	58	0,0010	209	0,002
55	13000	1,13	1	1,04	0,047	60	0,0000	210	0,000
57,5	13000	1,14	1	1,04	0,046	61	0,0000	211	0,000
60	13000	1,15	1	1,05	0,046	63	0,0000	212	0,000
62,5	13000	1,16	1	1,05	0,045	65	0,0000	213	0,000
65	13000	1,16	1	1,05	0,044	67	0,0000	214	0,000
67,5	13000	1,17	1	1,06	0,044	69	0,0000	214	0,000
70	13000	1,18	1	1,06	0,043	71	0,0000	215	0,000
72,5	13000	1,18	1	1,06	0,043	72	0,0000	216	0,000
75	13000	1,19	1	1,07	0,042	74	0,0000	217	0,000
77,5	13000	1,19	1	1,07	0,042	76	0,0000	217	0,000
80	13000	1,20	1	1,07	0,041	77	0,0000	218	0,000
82,5	13000	1,20	1	1,08	0,041	78	0,0000	219	0,000
85	13000	1,21	1	1,08	0,040	80	0,0000	219	0,000
87,5	13000	1,21	1	1,08	0,040	81	0,0000	220	0,000
90	13000	1,21	1	1,09	0,039	83	0,0000	220	0,000
92,5	13000	1,22	1	1,09	0,039	84	0,0000	221	0,000
95	13000	1,22	1	1,09	0,038	85	0,0000	222	0,000
97,5	13000	1,22	1	1,10	0,038	87	0,0000	222	0,000
100	13000	1,22	1	1,10	0,037	88	0,0000	223	0,000
102,5	13000	1,22	1	1,11	0,037	89	0,0000	224	0,000
105	13000	1,22	1	1,11	0,037	90	0,0000	225	0,000
107,5	13000	1,23	1	1,11	0,036	91	0,0000	225	0,000
110	13000	1,23	1	1,12	0,036	92	0,0000	226	0,000
112,5	13000	1,23	1	1,12	0,036	93	0,0000	227	0,000
115	13000	1,23	1	1,12	0,035	94	0,0000	227	0,000
117,5	13000	1,23	1	1,13	0,035	95	0,0000	228	0,000
120	13000	1,23	1	1,13	0,034	96	0,0000	228	0,000
122,5	13000	1,22	1	1,13	0,034	97	0,0000	229	0,000
125	13000	1,22	1	1,14	0,034	98	0,0000	230	0,000
127,5	13000	1,22	1	1,14	0,033	99	0,0000	230	0,000
130	13000	1,22	1	1,15	0,033	99	0,0000	232	0,000
132,5	13000	1,22	1	1,15	0,033	100	0,0000	232	0,000
135	13000	1,22	1	1,15	0,032	101	0,0000	233	0,000
137,5	13000	1,21	1	1,16	0,032	102	0,0000	234	0,000
140	13000	1,21	1	1,16	0,032	102	0,0000	234	0,000
142,5	13000	1,21	1	1,17	0,031	103	0,0000	235	0,000
145	13000	1,20	1	1,17	0,031	104	0,0000	236	0,000
147,5	13000	1,20	1	1,18	0,031	104	0,0000	236	0,000
150	13000	1,20	1	1,18	0,030	105	0,0000	237	0,000
5	23000	0,29	0						
7,5	23000	0,29	0						
10	23000	0,29	1	0,49	0,038	8	0,2998	172	0,988

p_1	Q	FR_theory	SS	FR_computed	m_dot	dT_subcooling	x_4	T_1	L_biphase
12,5	23000	0,47	1	0,51	0,043	12	0,2549	178	0,826
15	23000	0,54	1	0,53	0,049	15	0,2186	183	0,713
17,5	23000	0,59	1	0,55	0,054	18	0,1896	187	0,623
20	23000	0,63	1	0,57	0,059	21	0,1655	191	0,551
22,5	23000	0,66	1	0,59	0,063	23	0,1468	195	0,493
25	23000	0,69	1	0,62	0,069	26	0,1244	198	0,432
27,5	23000	0,71	1	0,64	0,075	28	0,1052	201	0,378
30	23000	0,73	1	0,67	0,081	29	0,0885	204	0,328
32,5	23000	0,75	1	0,69	0,087	31	0,0739	207	0,282
35	23000	0,77	1	0,72	0,092	33	0,0626	210	0,243
37,5	23000	0,78	1	0,76	0,099	34	0,0471	212	0,190
40	23000	0,80	1	0,80	0,104	36	0,0361	214	0,147
42,5	23000	0,81	1	0,83	0,105	38	0,0300	216	0,120
45	23000	0,82	1	0,86	0,104	39	0,0261	218	0,101
47,5	23000	0,83	1	0,87	0,103	40	0,0238	220	0,088
50	23000	0,84	1	0,89	0,101	42	0,0218	222	0,077
52,5	23000	0,85	1	0,90	0,099	43	0,0209	224	0,071
55	23000	0,86	1	0,92	0,097	44	0,0183	225	0,059
57,5	23000	0,87	1	0,92	0,095	46	0,0182	227	0,056
60	23000	0,88	1	0,93	0,093	47	0,0176	229	0,052
62,5	23000	0,88	1	0,95	0,091	48	0,0162	230	0,046
65	23000	0,89	1	0,95	0,089	49	0,0163	232	0,044
67,5	23000	0,90	1	0,96	0,087	50	0,0146	233	0,038
70	23000	0,90	1	0,96	0,086	51	0,0154	235	0,039
72,5	23000	0,91	1	0,97	0,084	52	0,0144	236	0,034
75	23000	0,91	1	0,97	0,083	53	0,0146	238	0,034
77,5	23000	0,92	1	0,98	0,081	54	0,0142	239	0,032
80	23000	0,92	1	0,99	0,079	55	0,0130	240	0,028
82,5	23000	0,92	1	0,99	0,079	55	0,0126	242	0,027
85	23000	0,93	1	1,00	0,077	56	0,0131	243	0,026
87,5	23000	0,93	1	1,01	0,076	57	0,0112	244	0,022
90	23000	0,93	1	1,01	0,074	58	0,0110	245	0,021
92,5	23000	0,94	1	1,01	0,074	58	0,0113	247	0,021
95	23000	0,94	1	1,01	0,072	59	0,0115	248	0,020
97,5	23000	0,94	1	1,02	0,071	60	0,0103	249	0,018
100	23000	0,94	1	1,03	0,070	61	0,0093	250	0,015
102,5	23000	0,94	1	1,03	0,070	61	0,0102	252	0,017
105	23000	0,94	1	1,03	0,069	62	0,0095	253	0,015
107,5	23000	0,94	1	1,04	0,068	62	0,0090	254	0,014
110	23000	0,94	1	1,04	0,067	63	0,0086	255	0,013
112,5	23000	0,94	1	1,04	0,066	63	0,0085	256	0,012
115	23000	0,94	1	1,05	0,065	64	0,0085	257	0,012
117,5	23000	0,94	1	1,05	0,065	64	0,0081	259	0,011
120	23000	0,94	1	1,06	0,064	65	0,0061	260	0,008
122,5	23000	0,94	1	1,06	0,063	65	0,0065	261	0,008
125	23000	0,94	1	1,07	0,063	66	0,0047	262	0,006
127,5	23000	0,94	1	1,07	0,062	66	0,0054	263	0,007
130	23000	0,94	1	1,07	0,061	67	0,0037	264	0,004
132,5	23000	0,94	1	1,08	0,061	67	0,0020	265	0,002
135	23000	0,94	1	1,08	0,060	67	0,0032	266	0,004
137,5	23000	0,93	1	1,08	0,060	67	0,0032	268	0,004
140	23000	0,93	1	1,09	0,059	68	0,0017	269	0,002
142,5	23000	0,93	1	1,09	0,059	68	0,0002	270	0,000
145	23000	0,92	1	1,09	0,058	68	0,0000	271	0,000
147,5	23000	0,92	1	1,10	0,058	69	0,0000	272	0,000
150	23000	0,92	1	1,10	0,057	70	0,0000	272	0,000
5	33000	0,29	0						
7,5	33000	0,29	0						
10	33000	0,29	1	0,42	0,030	0	0,5476	172	1,000
12,5	33000	0,29	0						
15	33000	0,29	0						
17,5	33000	0,29	1	0,43	0,037	0	0,4606	201	1,000
20	33000	0,39	1	0,49	0,039	5	0,4464	207	0,977
22,5	33000	0,45	1	0,50	0,041	8	0,4167	210	0,911
25	33000	0,50	1	0,51	0,043	11	0,3950	213	0,855

p_1	Q	FR_theory	SS	FR_computed	m_dot	dT_subcooling	x_4	T_1	L_biphase
27,5	33000	0,53	1	0,52	0,045	13	0,3798	216	0,809
30	33000	0,55	1	0,53	0,046	15	0,3659	219	0,770
32,5	33000	0,58	1	0,54	0,048	17	0,3466	221	0,730
35	33000	0,60	1	0,55	0,049	19	0,3388	224	0,701
37,5	33000	0,61	1	0,56	0,051	21	0,3253	226	0,669
40	33000	0,63	1	0,57	0,052	22	0,3125	228	0,640
42,5	33000	0,64	1	0,58	0,053	24	0,3039	230	0,615
45	33000	0,66	1	0,59	0,055	25	0,2924	232	0,591
47,5	33000	0,67	1	0,59	0,056	27	0,2846	234	0,569
50	33000	0,68	1	0,60	0,057	28	0,2773	236	0,550
52,5	33000	0,69	1	0,61	0,058	29	0,2702	238	0,532
55	33000	0,70	1	0,62	0,059	30	0,2635	240	0,515
57,5	33000	0,70	1	0,63	0,060	31	0,2541	241	0,493
60	33000	0,71	1	0,64	0,061	32	0,2479	243	0,478
62,5	33000	0,72	1	0,64	0,061	33	0,2448	245	0,466
65	33000	0,73	1	0,65	0,062	35	0,2360	246	0,447
67,5	33000	0,73	1	0,66	0,063	35	0,2333	248	0,436
70	33000	0,74	1	0,67	0,064	36	0,2247	249	0,419
72,5	33000	0,74	1	0,68	0,064	37	0,2223	251	0,409
75	33000	0,75	1	0,69	0,065	38	0,2141	252	0,393
77,5	33000	0,75	1	0,69	0,065	39	0,2145	254	0,386
80	33000	0,76	1	0,70	0,066	40	0,2065	255	0,371
82,5	33000	0,76	1	0,70	0,066	40	0,2098	257	0,367
85	33000	0,76	1	0,71	0,067	41	0,2018	258	0,353
87,5	33000	0,77	1	0,72	0,067	41	0,2028	260	0,348
90	33000	0,77	1	0,73	0,067	42	0,1976	261	0,336
92,5	33000	0,77	1	0,74	0,068	43	0,1925	262	0,324
95	33000	0,77	1	0,74	0,067	43	0,1963	264	0,323
97,5	33000	0,77	1	0,75	0,068	44	0,1913	265	0,312
100	33000	0,78	1	0,76	0,068	45	0,1862	266	0,301
102,5	33000	0,78	1	0,77	0,068	45	0,1839	267	0,292
105	33000	0,78	1	0,77	0,068	46	0,1883	269	0,292
107,5	33000	0,78	1	0,78	0,068	46	0,1833	270	0,282
110	33000	0,78	1	0,79	0,068	47	0,1811	271	0,275
112,5	33000	0,78	1	0,79	0,068	47	0,1859	273	0,275
115	33000	0,78	1	0,79	0,068	47	0,1839	274	0,268
117,5	33000	0,78	1	0,80	0,068	48	0,1819	275	0,261
120	33000	0,78	1	0,81	0,068	48	0,1799	276	0,254
122,5	33000	0,78	1	0,81	0,067	48	0,1884	278	0,258
125	33000	0,78	1	0,82	0,067	49	0,1866	279	0,252
127,5	33000	0,78	1	0,82	0,067	49	0,1848	280	0,246
130	33000	0,77	1	0,83	0,067	50	0,1830	281	0,239
132,5	33000	0,77	1	0,84	0,066	50	0,1846	282	0,236
135	33000	0,77	1	0,83	0,065	50	0,1944	284	0,241
137,5	33000	0,77	1	0,84	0,065	50	0,1929	285	0,235
140	33000	0,77	1	0,85	0,065	50	0,1950	286	0,232
142,5	33000	0,76	1	0,85	0,065	51	0,1935	287	0,226
145	33000	0,76	1	0,85	0,064	51	0,2048	289	0,232
147,5	33000	0,76	1	0,86	0,063	51	0,2075	290	0,229
150	33000	0,75	1	0,86	0,063	51	0,2063	291	0,224
5	43000	0,29	0						
7,5	43000	0,29	0						
10	43000	0,29	1	0,42	0,026	0	0,8099	172	1,000
12,5	43000	0,29	0						
15	43000	0,29	1	0,42	0,031	0	0,7054	193	1,000
17,5	43000	0,29	1	0,42	0,033	0	0,6731	201	1,000
20	43000	0,29	1	0,42	0,035	0	0,6530	208	1,000
22,5	43000	0,29	0						
25	43000	0,29	0						
27,5	43000	0,29	0						
30	43000	0,31	0						
32,5	43000	0,39	0						
35	43000	0,43	0						
37,5	43000	0,46	1	0,44	0,042	0	0,5933	244	1,000
40	43000	0,48	1	0,50	0,043	4	0,5806	246	0,972

p_1	Q	FR_theory	SS	FR_computed	m_dot	dT_subcooling	x_4	T_1	L_biphase
42,5	43000	0,50	1	0,51	0,043	6	0,5752	248	0,944
45	43000	0,51	1	0,52	0,044	7	0,5636	250	0,919
47,5	43000	0,53	1	0,52	0,045	9	0,5590	252	0,896
50	43000	0,54	1	0,53	0,046	10	0,5484	254	0,876
52,5	43000	0,55	1	0,53	0,046	12	0,5414	255	0,852
55	43000	0,56	1	0,54	0,047	13	0,5377	257	0,835
57,5	43000	0,57	1	0,54	0,047	14	0,5342	259	0,819
60	43000	0,58	1	0,55	0,048	15	0,5310	261	0,804
62,5	43000	0,59	1	0,55	0,048	16	0,5248	262	0,786
65	43000	0,60	1	0,56	0,049	17	0,5220	264	0,773
67,5	43000	0,60	1	0,56	0,049	18	0,5161	265	0,757
70	43000	0,61	1	0,57	0,050	19	0,5137	267	0,746
72,5	43000	0,62	1	0,57	0,050	20	0,5140	268	0,732
75	43000	0,62	1	0,58	0,050	20	0,5119	270	0,722
77,5	43000	0,63	1	0,58	0,051	21	0,5066	271	0,709
80	43000	0,63	1	0,59	0,051	22	0,5107	273	0,702
82,5	43000	0,63	1	0,59	0,051	23	0,5056	274	0,689
85	43000	0,64	1	0,59	0,051	23	0,5100	276	0,683
87,5	43000	0,64	1	0,60	0,052	24	0,5051	277	0,671
90	43000	0,64	1	0,60	0,052	24	0,5099	279	0,666
92,5	43000	0,65	1	0,61	0,052	25	0,5111	280	0,657
95	43000	0,65	1	0,61	0,052	26	0,5065	281	0,646
97,5	43000	0,65	1	0,62	0,052	26	0,5118	283	0,643
100	43000	0,65	1	0,62	0,052	27	0,5133	284	0,634
102,5	43000	0,65	1	0,62	0,052	27	0,5190	286	0,631
105	43000	0,66	1	0,63	0,053	27	0,5148	287	0,622
107,5	43000	0,66	1	0,63	0,053	28	0,5167	288	0,615
110	43000	0,66	1	0,64	0,053	28	0,5231	290	0,612
112,5	43000	0,66	1	0,64	0,053	29	0,5253	291	0,605
115	43000	0,66	1	0,64	0,053	29	0,5277	292	0,599
117,5	43000	0,66	1	0,65	0,053	29	0,5347	294	0,597
120	43000	0,66	1	0,65	0,053	29	0,5375	295	0,591
122,5	43000	0,66	1	0,66	0,053	30	0,5404	296	0,585
125	43000	0,65	1	0,66	0,053	30	0,5483	298	0,584
127,5	43000	0,65	1	0,66	0,053	30	0,5516	299	0,579
130	43000	0,65	1	0,67	0,053	30	0,5551	300	0,573
132,5	43000	0,65	1	0,67	0,053	30	0,5638	302	0,573
135	43000	0,65	1	0,67	0,053	31	0,5678	303	0,568
137,5	43000	0,65	1	0,68	0,053	31	0,5721	304	0,563
140	43000	0,64	1	0,68	0,053	31	0,5818	306	0,563
142,5	43000	0,64	1	0,69	0,053	31	0,5866	307	0,558
145	43000	0,64	1	0,69	0,053	31	0,5916	308	0,553
147,5	43000	0,63	1	0,69	0,053	31	0,6025	310	0,554
150	43000	0,63	1	0,70	0,053	31	0,6082	311	0,549

- **p_1** [**bar**]: pressure at point 1;
- **Q** [**W**]: steam generator power;
- **FR_theory**: FR computed using the correlation presented by Santini et al.;
- **SS** [**logical**]: 1 if the algorithm found a steady state equilibrium, 0 otherwise;
- **FR_computed**: FR computed with the actual mass resulting from the simulation;
- **m_dot** [**kg/s**]: mass flow rate;
- **dT_subcooling** [**°C**]: subcooling of the fluid exiting the condenser;
- **x_4**: quality of the steam at the inlet of the condenser;
- **T_1** [**°C**]: temperature at point 1;
- **L_biphase** [**m**]: length of the condenser where the fluid is a two-phase mixture.